

Supplemental Materials

Polysulfide polyurethane-urea-based dielectric composites with CeO₂ loaded MXene exhibiting high self-healing efficiency

Ying-Jie Ma, Jing-Wen Wang *, Guo-Chao Zhuang, Yang Zhang, Zi-Long Zhang,
Ming-Yue Zhang, Guang-Bin Ji *

*College of Materials Science and Technology, Nanjing University of Aeronautics and
Astronautics, Nanjing 210016, P. R. China*

*Corresponding Author:

Prof. Dr. Jing-Wen Wang, E-mail: wjw_msc@nuaa.edu.cn

Prof. Dr. Guang-Bin Ji, E-mail: gbi@nuaa.edu.cn

Measurement and Characteristic:

Fourier transform infrared spectra (FT-IR) were recorded with Nicolet iS50 (Thermo Fisher) with a scanning range from 400 to 4000 cm^{-1} . The ^1H nuclear magnetic resonance (^1H -NMR) spectrum of PSPU was recorded using a Bruker WM300 (Germany) spectrometer with deuterated dimethyl sulfoxide as the solvent and the internal standard. X-ray photoelectron spectroscopy (XPS) results were documented with a K-Alpha+ spectrometer (Thermo Scientific) equipped with a monochromatic Al $K\alpha$ excitation source. X-ray diffraction (XRD) patterns were scanned on Ultima IV with Cu $K\alpha$ radiation from 5° to 80° . The microstructures of MXene, $\text{CeO}_2@\text{MXene}$, MXene/PSPU and $\text{CeO}_2@\text{MXene}/\text{PSPU}$ composites were observed on the Scanning Electron Microscope (SEM, JSM-6510). Before the SEM measurement, the film samples were fractured in liquid nitrogen to obtain the fracture surfaces, and samples were sputtered with gold. The microstructure of MXene was observed using Transmission Electron Microscope (TEM, JEM-2100). TEM sample preparation: a proper amount of sample powder is fully dispersed in ethanol, and then dropped onto the copper mesh with a pipette, and fully dried under an infrared light. The direct current (DC) conductivities were recorded with a digital four-point probe (kdy-1 from Guangzhou Kund Technology Co., Ltd). Breakdown strength experiment was performed using an electric breakdown tester (ZJC-50kV, Beijing Zhide Innovation Instrument and Equipment Co., Ltd.) in a silicone oil bath. Tensile tests were performed using a universal testing machine (XWW-5A, China) at room temperature in a 2 mm/min tensile mode. All samples were made according to ISO 527 test standard using

a dumbbell-shaped PTFE mold 5A. Dielectric measurements were carried out with a HP 4294A precision impedance analyzer (Agilent) in the frequency from 10^2 Hz to 10^6 Hz at room temperature, and the tested composite films were coated with circular carbon paste electrodes of 2 mm diameter on the both sides of each sample before measuring dielectric property. The dielectric constant was calculated according to the following equation:¹

$$\varepsilon_r = \frac{Cd}{A\varepsilon_0} \quad (\text{S-1})$$

where C , ε_0 , d , S are the tested capacitance, the vacuum permittivity, the thickness of the measured composite films, and the area of the electrode painted on the composite films.

Preparation of MXene

MXene nanosheet was obtained through a two steps method of the etching and delamination according to the previous reports.^{2,3} Specifically, 1 g LiF and 10 mL of 9 mol/L HCl were mixed in a three-neck round bottom flask and stirred magnetically for 10 min, then 1 g Ti_3AlC_2 powder was added into the flask, followed by stirring for 24 h at 35 °C. Afterwards, the mixture was centrifuged at 3500 rpm to obtain the precipitate and washed with deionized water until the pH value of the supernatants exceeded 6. Finally, the settled powders ($\text{Ti}_3\text{C}_2\text{T}_x$) were dried at room temperature for 24 h. The obtained multilayer $\text{Ti}_3\text{C}_2\text{T}_x$ powder (1 g) and 10 mL DMSO were mixed at a three-neck round bottom flask and stirred for 12 h at room temperature. Next 50 mL deionized water was added, accompanied with centrifugation at 3500 rpm for 10 min. The obtained precipitate was dispersed into 200 mL deionized water, and ultrasonicated

intermittently for 2 h at N₂ atmosphere. Finally, the mixture was centrifuged at 3500 rpm for 1 h. The filter cake acquired from vacuum filtration was placed in a vacuum oven for 24 h at 50 °C to obtain MXene.

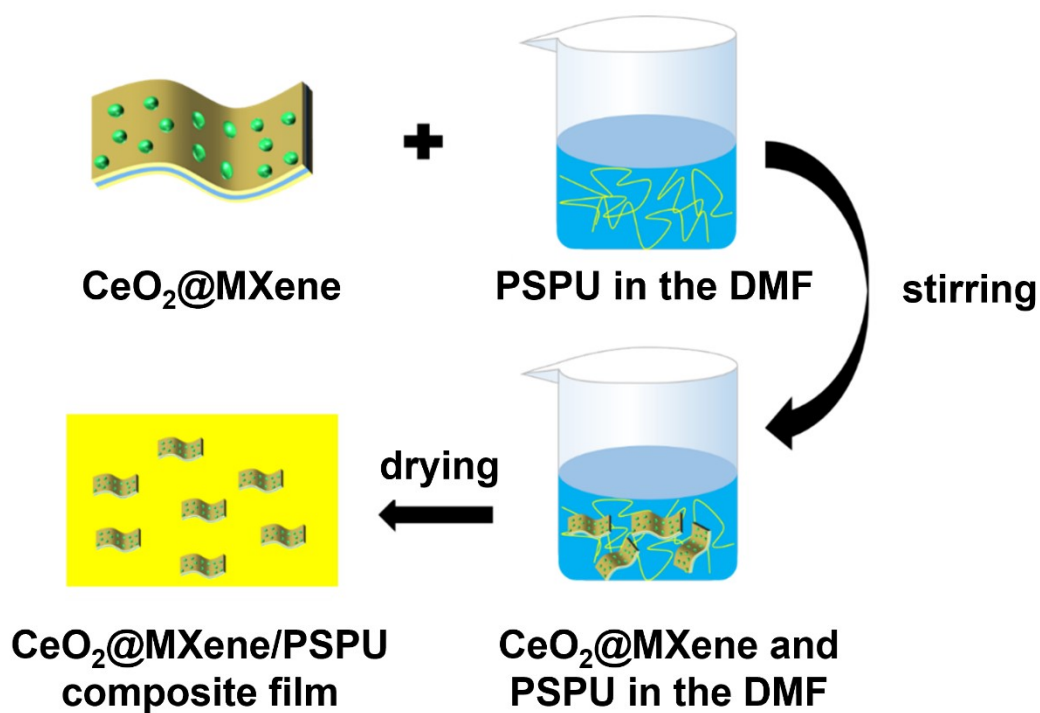


Figure S1. The fabrication route of CeO₂@MXene/PSPU composite film.

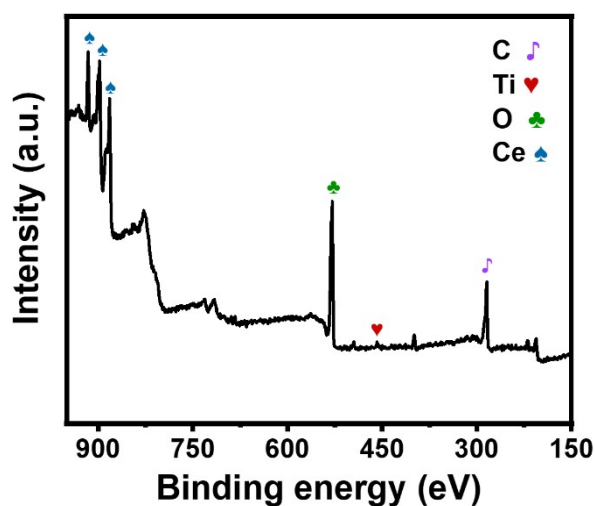


Figure S2. XPS spectrum of CeO₂@MXene.

Figure S3 presents the fracture sections of MXene/PSPU (a, b) and

CeO₂@MXene/PSPU (c, d) composites, respectively. It can be seen that in the MXene/PSPU composite, the filler has obvious agglomeration and a rougher surface in the quenched section. In contrast, the fillers in the CeO₂@MXene/PSPU composites are tightly bound to the matrix and have better dispersion. This indicates that the loading of CeO₂ is crucial to enhance the compatibility between MXene nanosheets and PSPU. As can be seen from Figure S3e and S3f, benefiting from the presence of dynamic disulfide and hydrogen bonding networks in PSPU, CeO₂@MXene with multiple dynamic interactions can synergistically provide a higher probability of reconstitution when the molecular chains are reentangled in the damaged region.⁴ Consequently, the presence of interfacial interactions between CeO₂@MXene and PSPU matrix heightens the self-healing efficiency of CeO₂@MXene/PSPU composites.

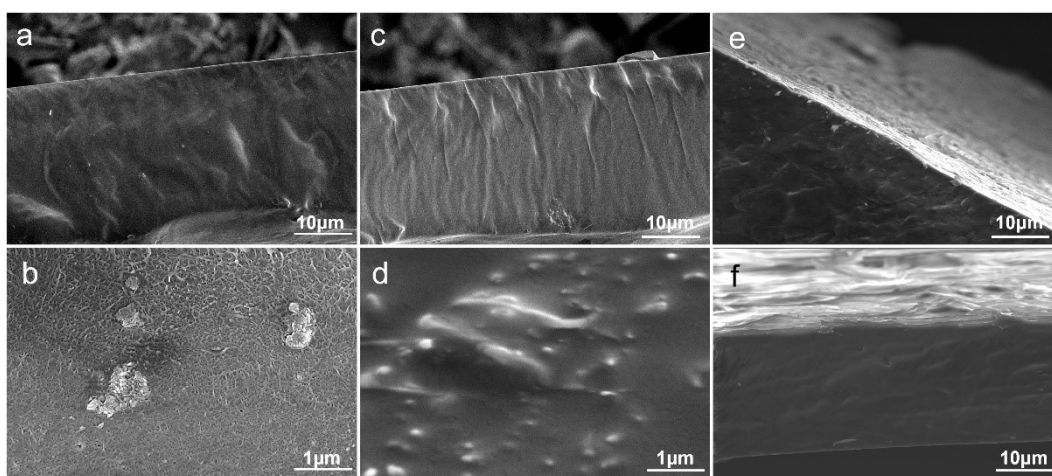


Figure S3. SEM images of the fracture sections of MXene/PSPU (a, b) and CeO₂@MXene/PSPU (c, d). SEM images of the damaged area of CeO₂@MXene/PSPU composites after healing at 110 °C for 3 h (e, f).

The breakdown strength of the MXene/PSPU and CeO₂@MXene/PSPU composites with different filler contents is shown in Figure S4. It is apparent that the breakdown strength of both declines with increasing filler content, as a natural

consequence of the introduction of conductive fillers. However, the overall breakdown strength of the CeO₂@MXene/PSPU composite is higher than that of MXene/PSPU, perhaps because CeO₂ acts as an insulating layer to hinder the spread of electrical tree branches and the excellent compatibility between CeO₂@MXene and the PSPU matrix averts surface discharge and flashover of the material.⁵

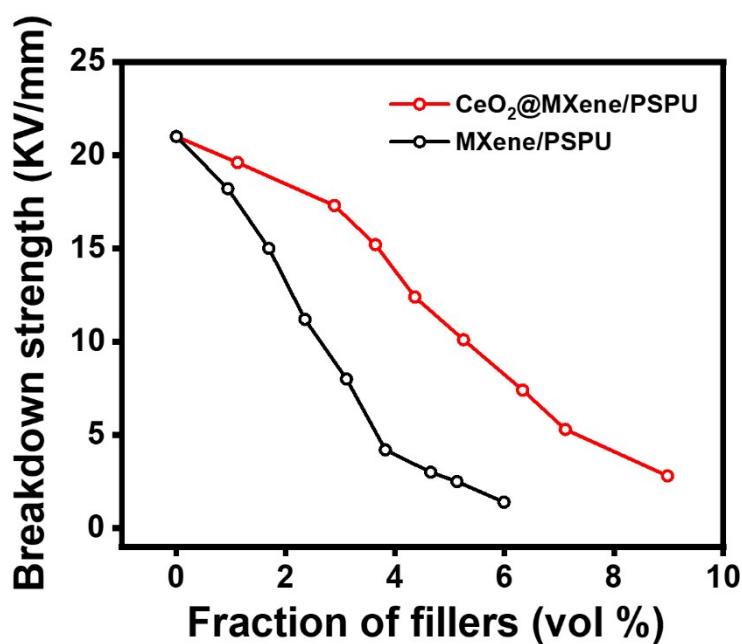


Figure S4. Trend of breakdown strength of MXene/PSPU and CeO₂@MXene/PSPU composites with filler content.

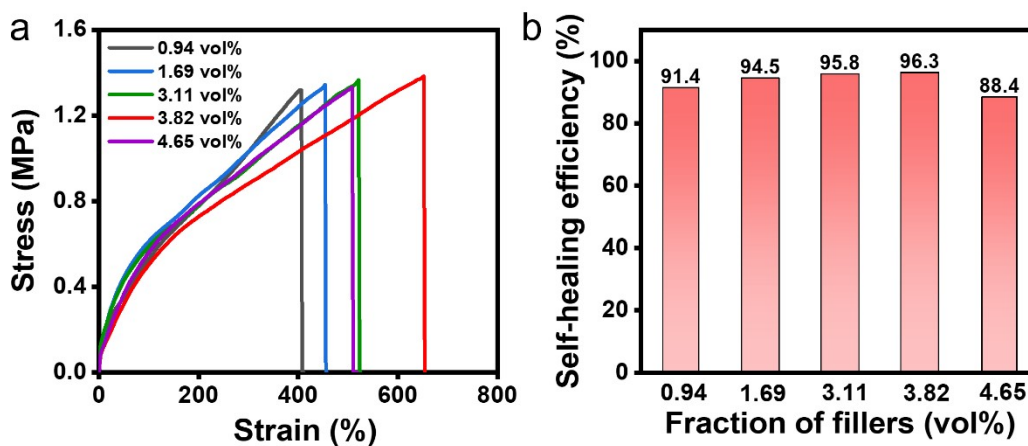


Figure S5. (a) Stress-strain plots of MXene/PSPU composite films at different filler contents after heating at 110 °C for 3 h. (b) Healing efficiency of damaged MXene/PSPU composite films at different filler contents after 3 h of healing at 110 °C.

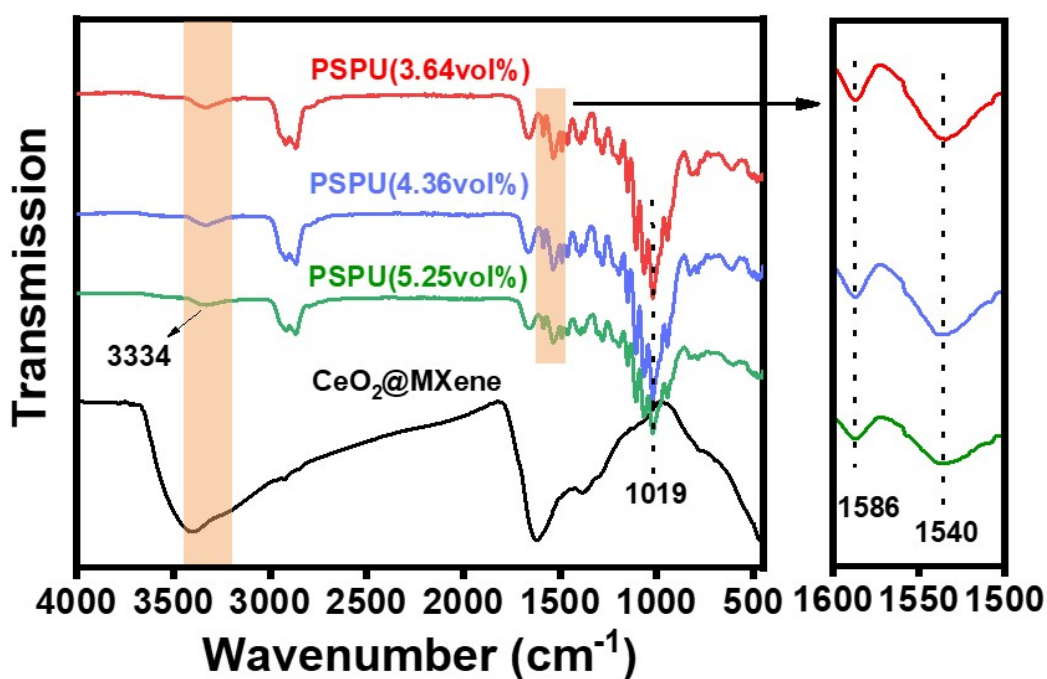


Figure S6. FT-IR spectra of CeO₂@MXene and CeO₂@MXene/PSPU composites with different filler contents, where the CeO₂@MXene/PSPU composite with 5.25 vol% of filler is abbreviated as PSPU (5.25 vol%) and the others are similarly abbreviated.

Table S1. Self-healing efficiency of PSPU, MXene/PSPU and CeO₂@MXene/PSPU composites.

Samples	Filler content (vol%)	T ₁ (MPa)	T ₀ (MPa)	Self-healing efficiency (%)
PSPU	-	1.36	1.44	95
	0.94	1.23	1.31	91.4
	1.69	1.26	1.34	94.5
MXene/PSPU	3.11	1.30	1.36	95.8
	3.82	1.32	1.38	96.3
	4.65	1.17	1.33	88.4
	1.12	1.22	1.31	93.6
	2.89	1.31	1.37	95.7
CeO ₂ @MXene/PSPU	4.36	1.33	1.39	96.2
	5.25	1.35	1.38	97.9
	6.33	1.19	1.34	89

References

1. R. Pelrine, R. Kornbluh, P. Qibing and J. Joseph, *Science*, 2000, **287**, 836-839.
2. L. Yao, Q. Gu and X. Yu, *ACS Nano*, 2021, **15**, 3228-3240.
3. G. Ge, Y. Z. Zhang, W. Zhang, W. Yuan, J. K. El-Demellawi, P. Zhang, E. Di Fabrizio, X. Dong and H. N. Alshareef, *ACS Nano*, 2021, **15**, 2698-2706.
4. T. Yimyai, D. Crespy and A. Pena-Francesch, *Adv Funct Mater*, 2023, **33**, 2213717.
5. C. Luo, J. Li, Z. Chen, J. Lin, L. Chen and S. He, *Mater Today Commun*, 2022, **31**, 103619.